Single-Doppler Velocity Retrieval of the Wind Field in a Tornadic Supercell Using Mobile, Phased-Array, Doppler Radar Data

YU-CHIENG LIOU

Department of Atmospheric Sciences, National Central University, Taoyuan, Taiwan

HOWARD B. BLUESTEIN

School of Meteorology, University of Oklahoma, Norman, Oklahoma

MICHAEL M. FRENCH

School of Marine and Atmospheric Sciences, Stony Brook University, State University of New York, Stony Brook, New York

ZACHARY B. WIENHOFF

School of Meteorology, University of Oklahoma, Norman, Oklahoma

(Manuscript received 9 January 2018, in final form 29 May 2018)

ABSTRACT

A three-dimensional data assimilation (3DVar) least squares–type single-Doppler velocity retrieval (SDVR) algorithm is utilized to retrieve the wind field of a tornadic supercell using data collected by a mobile, phased-array, Doppler radar [Mobile Weather Radar (MWR) 05XP] with very high temporal resolution (6 s). It is found that the cyclonic circulation in the hook-echo region can be successfully recovered by the SDVR algorithm. The quality of the SDVR analyses is evaluated by dual-Doppler syntheses using data collected by two mobile Doppler radars [Doppler on Wheels 6 and 7 (DOW6 and DOW7, respectively)]. A comparison between the SDVR analyses and dual-Doppler syntheses confirms the conclusion reached by an earlier theoretical analysis that because of the temporally discrete nature of the radar data, the wind speed retrieved by single-Doppler radar is always underestimated, and this underestimate occurs more significantly for the azimuthal (crossbeam) wind component than for the radial (along beam) component. However, the underestimate can be mitigated by increasing the radar data temporal resolution. When the radar data are collected at a sufficiently high rate, the azimuthal wind component may be overestimated. Even with data from a rapid scan, phased-array, Doppler radar, our study indicates that it is still necessary to calculate the SDVR in an optimal moving frame of reference. Finally, the SDVR algorithm's robustness is demonstrated. Even with a temporal resolution (2 min) much lower than that of the phased-array radar, the cyclonic flow structure in the hook-echo region can still be retrieved through SDVR using data observed by DOW6 or DOW7, although a difference in the retrieved fields does exist. A further analysis indicates that this difference is caused by the location of the radars.

1. Introduction

A Doppler radar can detect only the radial wind (V_r), which is the projection of the three-dimensional wind along the radar beam. The crossbeam wind components perpendicular to the radar beam are undetectable by a Doppler radar and need to be recovered by other means. When multiple-Doppler observations are not available, variational single-Doppler velocity retrieval (SDVR) techniques, first developed in the early 1990s, may be viable. These methods utilize data collected by single-Doppler radar to retrieve the unobserved transverse wind components and to produce a complete wind field without sacrificing the spatial resolution of the radar data. There are two different types of SDVR techniques: The first type adopts the four-dimensional data assimilation (4DVar) adjoint technique and requires a prognostic dynamic model. Methods belonging to this category include those used by Sun et al. (1991), Qiu and Xu (1992), Laroche and Zawadzki (1994), Xu et al. (1995), and

Corresponding author: Dr. Yu-Chieng Liou, tyliou@atm.ncu.edu.tw

DOI: 10.1175/JTECH-D-18-0004.1

Gao et al. (2001) among others. The second type uses 3DVar analysis, in which the unobservable crossbeam winds can be retrieved by satisfying certain prescribed constraints in the least squares sense. Examples can be found in Shapiro et al. (1995), Qiu and Xu (1996), Gao et al. (2006), and Qiu et al. (2006).

The method employed in this study belongs to the second type. It is based on an algorithm first developed by Zhang and Gal-Chen (1996, hereafter ZG96). In ZG96, the retrieval is performed in an ''optimal'' moving frame of reference so that the assumption of Lagrangian conservation for radar reflectivity is least violated. In ZG96, the moving speed of this reference frame is a constant and can be determined objectively under the frozen-turbulence hypothesis (Gal-Chen 1982). The performance of this method under the influence of observational errors, weightings, and other factors has been investigated by Lazarus et al. (1999). Liou (1999) modified this method by implementing more physical and mathematical constraints to improve the quality of the retrieved wind fields. Liou and Luo (2001) investigated the sensitivity of the SDVR results to the geometric locations of the radar, by designing an index to reveal the reliability of the retrieved flow field. Lazarus et al. (2001) developed a two-step approach in an attempt to apply the ZG96 algorithm to analyze a deep convective storm. For the same purpose, Liou (2007, hereafter L07) improved the method of ZG96 and Liou (1999) by letting the moving speed of the optimal reference frame become a function of the height rather than a constant, thereby making possible a better application for deep convection.

One major finding from Liou and Luo (2001) was that the single-Doppler retrieved radial wind speed was comparable to its actual value (can be obtained from multiple-Doppler syntheses if available). By contrast, the wind speed along the azimuthal direction retrieved by single-Doppler radar was always less than its true counterpart. Liou (2002, hereafter L02) used a simplified one-dimensional model and assumed that the SDVR was performed on a horizontal plane at the same level as the radar. He found that the noncontinuous radar observations were the dominant factor controlling the accuracy of the retrieved azimuthal wind speed. On the other hand, the retrieved wind speed along the radial direction was less influenced by the scanning rate. Given the scanning rate of a modern operational Doppler weather radar (4–8 min per volume scan), this wind speed underestimate turns out to be inevitable. Nevertheless, L02's theoretical analysis also shows that for a given data spatial resolution, the wind speed underestimate can be effectively mitigated if the temporal resolution of the radar data can be increased. In addition, L02 also predicts that if the radar scanning rate is fast enough, an overestimate of the azimuthal wind speed is even possible.

It should be pointed out that the findings and conclusions reached by Liou and Luo (2001) and L02 are based on simulated datasets produced by an idealized model and a simplified theoretical analysis, and have never been verified with real radar observations, mainly owing to the lack of proper radar data with sufficiently high temporal resolution.

In this study the radar data used for experiments were collected by two mobile Doppler radars and a mobile, phased-array, Doppler radar. The latter is able to conduct scans with a very short volume update time (~6 s), thus providing a good opportunity to verify the conclusions reached in previous theoretical studies. Therefore, the purposes of this research are to use real radar observations to (i) show the successful application of the L07 SDVR algorithm to reconstruct the complete wind field in a supercell, and to demonstrate the advantages of using a phased-array rapid scan radar to improve the quality of the retrievals; (ii) validate the conclusion from L02 that the retrieved wind speed is always underestimated, and it is the azimuthal (crossbeam) wind component rather than the radial (along beam) component that is underestimated more significantly; (iii) verify the prediction from the theoretical model of L02 that mitigation of the underestimation of the azimuthal wind speed or even overestimation can happen if the data from a Doppler radar are obtained at very high scanning rates; and (iv) demonstrate the robustness of the L07 algorithm by applying it to recover the flow field using data collected at a lower temporal resolution.

It is worth noting that Weygandt et al. (2002) applied a 3DVar-based SDVR algorithm to retrieve the wind field of a tornadic thunderstorm that occurred on 17 May 1981 near Arcadia, Oklahoma. The radar data used for their retrieval come from an S-band ground-based Doppler radar with a temporal resolution of approximately 4–5 min. The same case was also investigated by Gao et al. (2006) using a new single-Doppler retrieval method. Shapiro et al. (2003) designed a dynamic model for single-Doppler wind retrieval and tested their method with the rapid scan radar data. In addition, to investigate the impact of different time resolutions on the retrievals, they focused on examining the role played by a background constraint. However, the case they selected was a slow-moving cold front in Oklahoma, and the highest temporal resolution of their radar data was only 1 min. Qiu et al. (2013) utilized the data collected by an S-band phased-array radar (PAR)—the NOAA National Weather Radar Testbed—located at the National Weather Service, Norman, Oklahoma to investigate the performance of a new simple adjoint method in recovering the three-dimensional wind of a microburst event. The temporal resolution of their datasets was about 30 s. The ground-based velocity track display (GBVTD) technique developed by Lee et al. (1999) represents a different approach to recovering the flow structure of a

tornado using single-Doppler radar observations achieved by fitting the rotational flow with a series of periodical functions (e.g., Lee and Wurman 2005; Tanamachi et al. 2007). Thus, to the authors' knowledge, this current study is the first attempt to use a 3DVar-based SDVR algorithm and rapid scan, phased-array, Doppler radar data to recover the flow field of a tornadic supercell.

The rest of the manuscript is organized in the following way. Section 2 introduces the L07 SDVR algorithm. Section 3 describes the case and datasets selected for this research. The assessment of the quality of the SDVR results from the phased-array Mobile Weather Radar (MWR) 05XP is discussed in section 4. A discussion related to the wind speed underestimation and overestimation associated with radar data temporal resolution is presented in section 5. Even with phased-array rapid scan radar data, the necessity to conduct SDVR in an optimal moving frame of reference is demonstrated in section 6. The SDVR results obtained using Doppler on Wheels 6 (DOW6) and DOW7 data are shown in section 7, followed by a summary in section 8.

2. Methodology

The following is a brief introduction of the L07 algorithm, in which the moving speed of an optimal frame can vary with the height.

a. Estimate of the optimal moving speed

Radar observations at a given point are collected in a temporally discontinuous manner. Thus, the temporal derivative of the radar data may lead to large errors. Gal-Chen (1982) suggested that this type of error can be reduced if the computation is performed over an optimal moving frame in which the radar reflectivity is conserved as much as possible.

The total wind fields u, v, and w can be decomposed into

$$\begin{aligned} u &= U(z) + u' \\ v &= V(z) + v' \\ w &= w', \end{aligned} \tag{1}$$

where u', v', and w' are the perturbation winds; U and V denote the moving speed of an optimal frame and can be obtained by minimizing the following cost function:

$$J_M = \frac{1}{2}\int\left\{\left[\left(\frac{\partial\eta}{\partial t}\right) + U(z)\frac{\partial\eta}{\partial x} + V(z)\frac{\partial\eta}{\partial y}\right]^2 + \sigma\left[\frac{\partial^2 U(z)}{\partial z^2}\right]^2 + \left[\frac{\partial^2 V(z)}{\partial z^2}\right]^2\right\} dx\,dy\,dz\,dt. \tag{2}$$

In (2) η denotes the radar reflectivity, and the optimal moving speed is allowed to vary with height. It should be pointed out that in (1) and (2) the moving speed along the vertical direction is not considered, and the w in (1) contains the contributions from both air motion and terminal velocity of the precipitation particles. The latter can be estimated by an empirical formula using radar reflectivity measurements (e.g., Shapiro et al. 1995). The weighting coefficient σ is used to balance the magnitude of each term and is set to be 10^5 in this study. Note that Shapiro et al. (2010a,b) extended the concept of Gal-Chen (1982) by considering spatially variable advection correction of the radar data. Thus, in their formulation, the moving speeds U and V can also vary horizontally. However, this type of correction is not applied in the current study.

b. Estimation of the perturbation wind field

After obtaining the optimal advection speed of the moving frame, a new reference frame (x', y', z') is formulated as follows:

$$\begin{aligned} x' &= x - U(t - t_0) \\ y' &= y - V(t - t_0) \\ z' &= z, \end{aligned} \tag{3}$$

where t_0 is a reference time and is usually selected as the time of the middle of the radar scan(s). All the radar observational data are then interpolated onto this newly defined optimal moving reference frame using the procedure introduced in ZG96. The next step is to compute the perturbations of the wind field u', v', and w' by minimizing the following cost function J_p in a weak constraint form:

$$J_P = \frac{1}{2}\iiint(\beta_1 J_1 + \beta_2 J_2 + \beta_3 J_3 + \beta_4 J_4 + \beta_5 J_5)\,dx\,dy\,dz\,dt; \tag{4a}$$

$$J_1 = \left(\frac{\partial\eta'}{\partial t'} + u'\frac{\partial\eta'}{\partial x'} + v'\frac{\partial\eta'}{\partial y'} + w'\frac{\partial\eta'}{\partial z'}\right)^2, \tag{4b}$$

$$J_2 = \left(v'_r - u'\frac{x'}{r'} - v'\frac{y'}{r'} - w'\frac{z'}{r'}\right)^2, \tag{4c}$$

$$J_3 = \left(\frac{\partial u'}{\partial x'} + \frac{\partial v'}{\partial y'} + \frac{\partial w'}{\partial z'}\right)^2, \tag{4d}$$

$$J_4 = |\nabla \times \mathbf{V}|^2, \tag{4e}$$

$$J_5 = (\nabla_H^2 u')^2 + (\nabla_H^2 v')^2 + (\nabla_H^2 w')^2, \tag{4f}$$

$$r' = \sqrt{(x')^2 + (y')^2 + (z')^2}, \tag{4g}$$

$$\nabla_H^2 = \frac{\partial^2}{\partial x'^2} + \frac{\partial^2}{\partial y'^2}. \tag{4h}$$

In the aforementioned expression of the constraints from J_1 to J_5, the prime denotes that these variables are defined on the moving frame of reference. Equation (4b) states that the law of reflectivity conservation (including with respect to vertical motions) needs to be

satisfied as much as possible. Note that in some single-Doppler retrieval schemes, the radial wind is selected as a conserved tracer (e.g., Xu et al. 1994; Xu et al. 1995), but this is not applied in our algorithm. Equation (4c) represents the geometric relation between the radar-observed radial winds (v_r') and the retrieved wind perturbations (u', v', w'). The incompressible (Boussinesq) continuity equation is employed as shown in (4d). The term J_4 is a weak vorticity condition, and it is implemented to prevent ill conditioning and to help the convergence of the solution (Liou and Luo 2001). Constraint J_5 provides a higher-order spatial filter to remove noise. The weighting coefficients ($\beta_1 - \beta_5$) determine the relative importance among the constraints in a cost function, and they are estimated in a manner similar to Liou (1999).

After obtaining the perturbation wind fields (u', v', w'), they are added to the optimal moving speed (U, V) expressed in (1) to get the total wind fields (u, v, w).

3. Description of the case and datasets

The real case selected for this study was a tornadic supercell that occurred in Goshen County, Wyoming, around 2200 UTC 5 June 2009 during the second Verification of the Origins of Rotation in Tornadoes Experiment (VORTEX2), a field campaign with the scientific objectives of understanding the tornadic structure, tornadogenesis, and improvement of forecasting (Wurman et al. 2012). The radar data used for our numerical experiments came from two X-band Doppler mobile radars (DOW6 and DOW7) and the MWR-05XP. A quality control procedure is applied to dealiase the folded radial winds observed by these radars. Wurman et al. (2012) and Markowski et al. (2012) described in detail the characteristics of DOW6 and DOW7 and the dual-Doppler data collection and analysis. For a detailed introduction of the characteristics of MWR-05XP see Bluestein et al. (2010), while its applications in observing several supercells and tornadoes can be found in French et al. (2013, 2014, 2015). French et al. (2014) pointed out that a drawback to the MWR-05XP is the lack of truck levelers (at that time) and a functioning system to record radar tilt after 2008. Fortunately, the deployment site for this Goshen County supercell was a paved road without noticeable changes in elevation (French et al. 2013). According to the error analysis conducted in French et al. (2014, see their Fig. 2), the heights between the MWR-05XP SDVR results and the dual-Doppler syntheses may be slightly off, but the errors should not change the major conclusions reached in this study.

In this study the radial wind fields observed by MWR-05XP are selected to produce two sets of input radar data. Each dataset contains data from three radar scans centered at 2200:06 UTC but with two distinct temporal resolutions of 6 s and 3 min. Note that the 3-min resolution data are produced by resampling the 6-s resolution datasets. Under this experimental design, the impact of an extremely high radar scanning rate on the SDVR results can be explored. In contrast, the radar data from DOW6 and DOW7 were collected from 2200:00 UTC, with an update time of 2 min. The dual-Doppler syntheses made using data from DOW6 and DOW7 are utilized to assess the performance of the SDVR using MWR-05XP, as well as DOW6 and DOW7 alone. Note that the horizontal and vertical grid spacings of the retrievals and analyses are 0.5 and 0.25 km, respectively. Thus, the retrieved wind field can resolve a mesocyclone but not a tornado.

The dual-Doppler analyses in this study are performed using a variational-based method named Wind Synthesis System Using Doppler Measurements (WISSDOM; see Liou et al. 2016). This method can recover three-dimensional wind fields along the radar's baseline and is able to merge data collected by any number of radars. Detailed introductions and other advantages of WISSDOM can be found in Liou and Chang (2009) and Liou et al. (2012). It should be pointed out that although the dual-Doppler syntheses are treated as the "true" solution of the wind fields, they still contain errors as a result of various factors, such as nonsimultaneous radar scans, uncertainties in the assumption of the top and bottom boundary conditions of the flow fields, and so on.

4. Results of single-Doppler retrievals using MWR-05XP phased-array radar data

Figure 1 shows the relative locations of DOW6, DOW7, and MWR-05XP with respect to the supercell.[1] The analysis domain for the dual-Doppler synthesis by DOW6 and DOW7 and for the SDVR experiments by MWR-05XP covers an area of 20 km × 18 km, as illustrated in Fig. 2. Two single-Doppler retrieval experiments using MWR-05XP phased-array radar data, named SDPA6s and SDPA3m, respectively, are conducted in which the temporal resolutions of the input radial velocity data are 6 s and 3 min, respectively.

Figure 2 illustrates the retrieved horizontal wind fields at Z = 500 m AGL from dual-Doppler synthesis and experiments SDPA6s and SDPA3m. The radar reflectivity in Fig. 2a is a composited result using measurements from DOW6 and DOW7, while the reflectivity shown in Figs. 2b and 2c is from the phased-array radar MWR-05XP.

[1] See also Fig. 4 in Markowski et al. (2012).

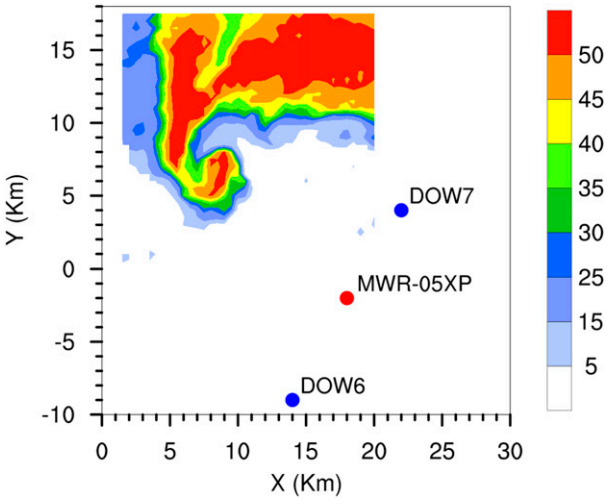

FIG. 1. The locations of DOW6, DOW7, and MWR-05XP during VORTEX2. The color shading indicates the composite radar reflectivity using DOW6 and DOW7 observations at 2200 UTC 5 Jun 2009.

Note that the reflectivity field shown in Fig. 2a is different from that in Figs. 2b and 2c, since the MWR-05XP transmitted lower power than DOW6 and DOW7.

The moving speed and direction of the optimal frame of reference at this layer from SDPA6s and SDPA3m are ($11.46\,m\,s^{-1}$, 277°) and ($11.50\,m\,s^{-1}$, 284°), respectively. It is shown that in both SDPA6s and SDPA3m, the retrieved flow structures are in agreement with those obtained from the dual-Doppler synthesis. The wind speed can exceed $20\,m\,s^{-1}$ in some locations, such as near the rear-flank gust front in SDPA6s. The successful recovery of the cyclonic circulation in the hook-echo region is particularly encouraging.

Figure 3 depicts the vertical vorticity ($\partial v/\partial x - \partial u/\partial y$) derived by dual-Doppler synthesis, by SDPA6s, and by SDPA3m. The computation of vorticity involves the first-order derivative of the winds; thus, it is highly sensitive to the accuracy of the retrieved wind field. It is found that both the location and magnitude of the maximum vorticity are well recovered by the SDVR algorithm. However, the SDPA6s overestimates the maximum vorticity by approximately 33%. Negative vorticity located to the south of the vortex is identified in Fig. 3a, and is recovered in Figs. 3b and 3c. However, the magnitude from the dual-Doppler synthesis is weaker than that retrieved by single-Doppler phased-array radar.

The vertical velocity (w) fields obtained by dual-Doppler syntheses, SDPA6s, and SDPA3m are displayed over a vertical cross section ($Y = 6$ km) and on a horizontal plane ($Z = 3$ km) in Figs. 4 and 5, respectively. The vertical cross section is selected so that it passes through the vortex center. The dual-Doppler syntheses in Figs. 4a and 5a show that significant downdrafts exist in the vortex center and vicinity, extending within a range of approximately 6 km, and are surrounded by updrafts. These features can be well retrieved in two SDVR experiments using 6-s and 3-min datasets. However, Figs. 4 and 5 also reveal that the w fields from SDVR are consistent with the dual-Doppler analyses only qualitatively. The vertical wind speed from SDVR is always weaker than its counterpart from dual-Doppler analysis.

The recovery of the w wind component is the most difficult and challenging part for SDVR. This is also true even for multiple-Doppler syntheses (Shapiro et al. 2009). One of the reasons is that as a result of the radar scan geometries, the contribution to the radial wind measurements from w is much less than that from the horizontal components u and v. This is a limitation to all wind analysis algorithms, without regard for single or multiple radar(s).

To examine the quality of the SDVR from radar data with different temporal resolutions, the dual-Doppler-synthesized and single-Doppler-retrieved Cartesian wind fields (u, v, w) were reprocessed to obtain the radial (V_r) and azimuthal (V_{az}) wind components viewed from the location of MWR-05XP using (5a) and (5b):

$$V_r = \frac{x}{r}u + \frac{y}{r}v + \frac{z}{r}w, \tag{5a}$$

$$V_{az} = \frac{y}{r\cos\theta}u - \frac{x}{r\cos\theta}v, \tag{5b}$$

$$r = \sqrt{x^2 + y^2 + z^2}, \tag{5c}$$

where x, y, and z are the coordinates of a given grid point with respect to the radar; and θ stands for the elevation angle. Note that V_{az} is the component unobservable by a Doppler radar.

In Fig. 6 the raw radial wind observed by MWR-05XP, and the dual-Doppler-synthesized and the SDVR-retrieved radial wind components obtained in experiments SDPA6s and SDPA3m are compared. It should be pointed out that the raw radial wind (Fig. 6a) is the wind field that would be matched by the retrieved V_r through variational adjustment in the SDVR algorithm. It can be seen that the spatial distribution of V_r obtained by SDVR (Figs. 6c and 6d) agrees quite well with the raw data, although the former is smoother. This is due to the implementation of the smoothness constraint in the SDVR algorithm as expressed by (4f). The magnitude of the retrieved V_r from the 6-s data (Fig. 6c) is comparable to the raw data. However, by comparing the peak values in the inbound and outbound regions, it is found that the retrieved V_r from the 3-min data (Fig. 6d) is weaker than the raw data. The dual-Doppler-synthesized radial wind (Fig. 6b) represents an independent way to verify the SDVR results. It is shown that the single-Doppler-retrieved radial winds

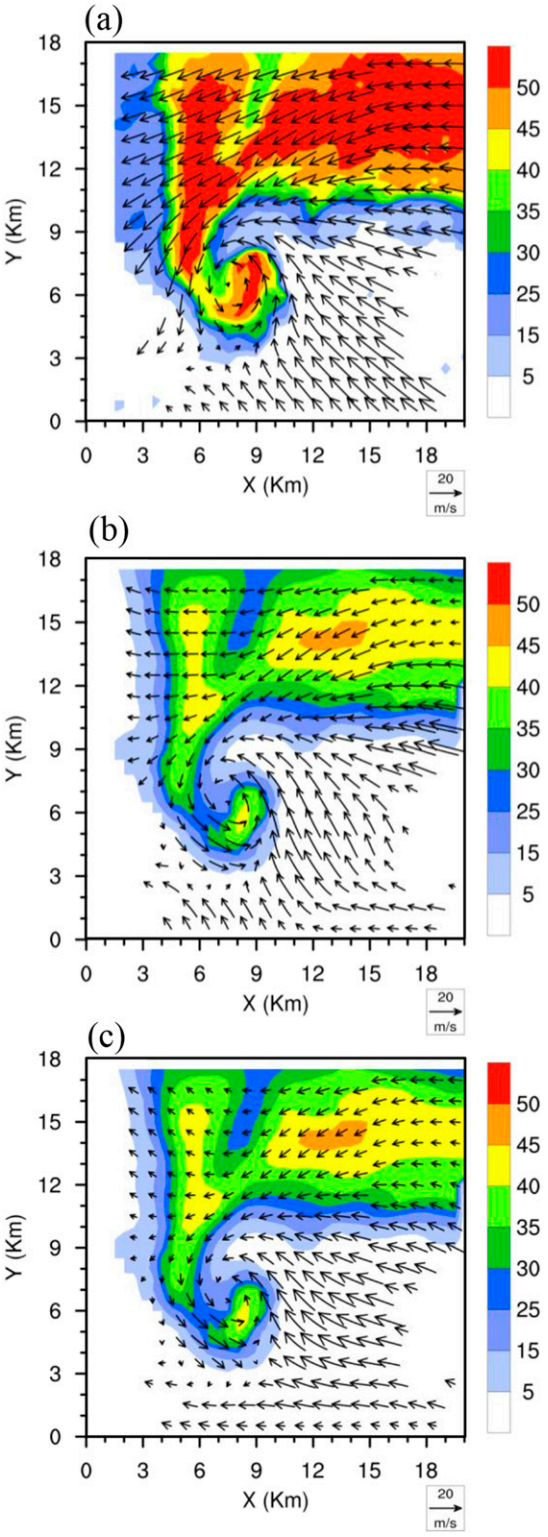

FIG. 2. The wind vectors for the Goshen County supercell on 5 June 2009 at $Z = 500$ m AGL from (a) dual-Doppler synthesis using DOW6 and DOW7 at 2200:00 UTC; SDVR by MWR-05XP at 2200:06 UTC with (b) SDPA6s and (c) SDPA3m. The color shading is radar reflectivity (dBZ).

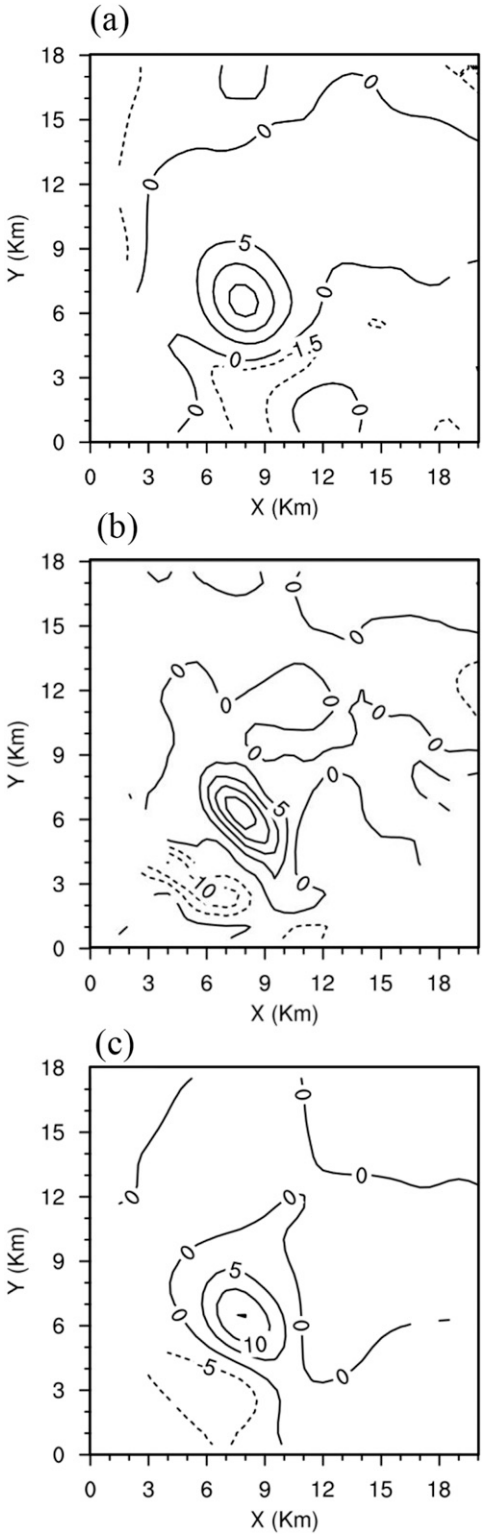

FIG. 3. As in Fig. 2, but for the vertical vorticity field ($s^{-1} \times 10^3$); positive (negative) values are denoted by solid (dashed) lines with an interval of $5.0 \times 10^{-3}\,s^{-1}$.

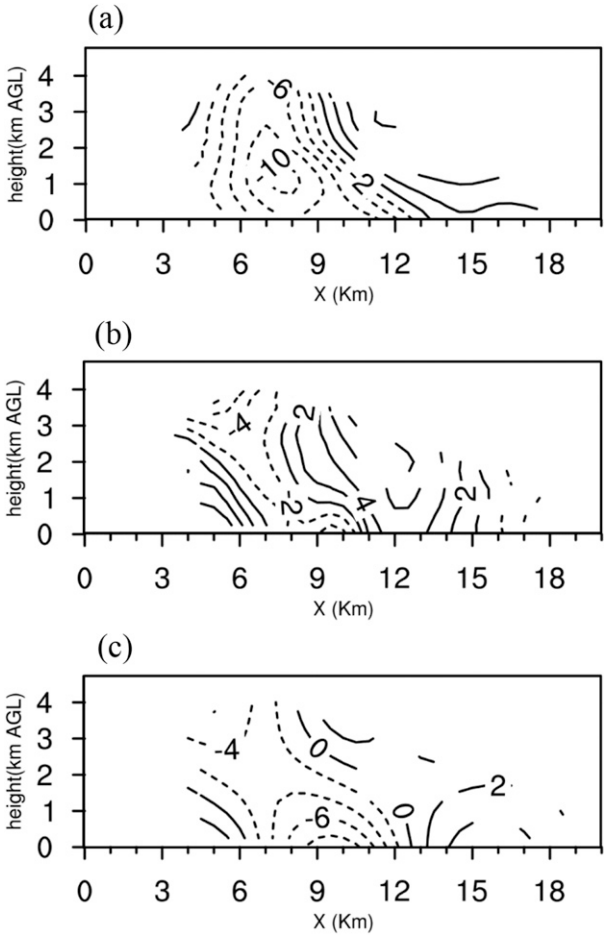

FIG. 4. The vertical velocity field over a vertical cross section at $Y = 6$ km from (a) dual-Doppler synthesis, and SDVR using (b) SDPA6s and (c) SDPA3m. The contour interval is 2.0 m s^{-1}.

obtained using data with 6-s and 3-min time resolutions are both consistent with the dual-Doppler-synthesized radial winds in terms of the spatial structure, except in the far southeastern part of the domain. However, the SDVR radial wind fields have denser gradients and stronger negative values compared with those from the dual-Doppler syntheses.

The retrieved azimuthal wind component from SDPA6s (Fig. 7b) is also in good agreement with the results of dual-Doppler synthesis (Fig. 7a). However, the retrieved V_{az} from SDPA3m (Fig. 7c), although still being similar in pattern, exhibits noticeable differences from the true solution in terms of its smaller magnitude.

A quantitative comparison is accomplished by computing the two-dimensional spatial correlation coefficient (SCC) and root-mean-square error (RMSE) at different altitudes. The results are shown only up to 1.5 km AGL, since above this height the dual-Doppler coverage by DOW6 and DOW7 drops to below 60% of the analysis area. In Fig. 8 it is seen that for the retrieved radial winds,

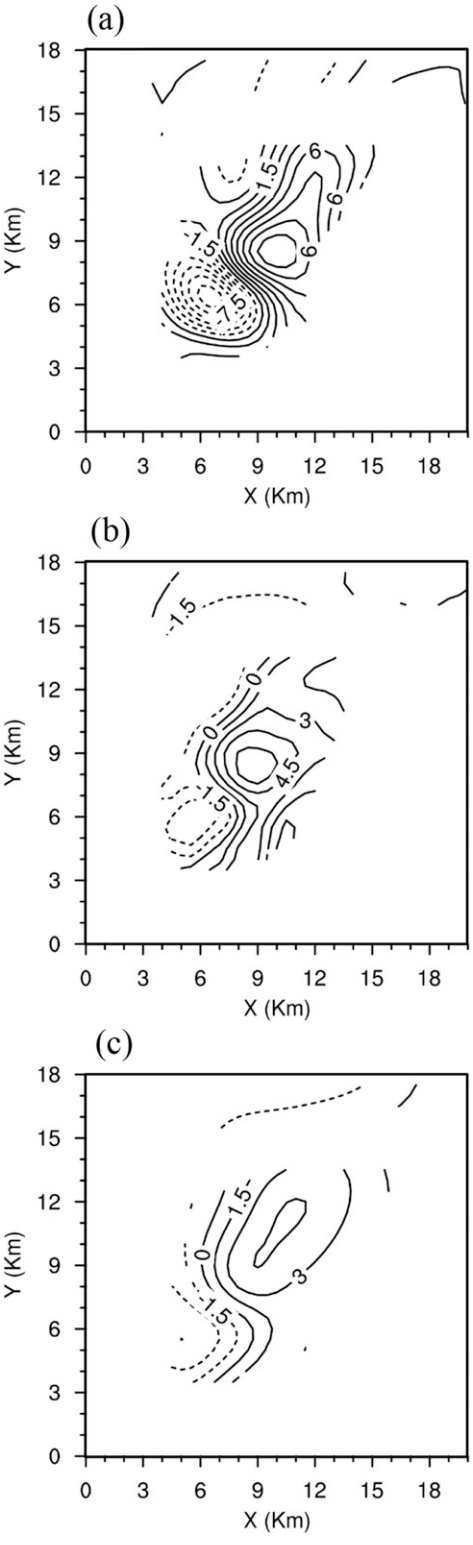

FIG. 5. As in Fig. 4, but for the vertical velocity field on a horizontal plane at $Z = 3$ km. The contour interval is 1.5 m s^{-1}.

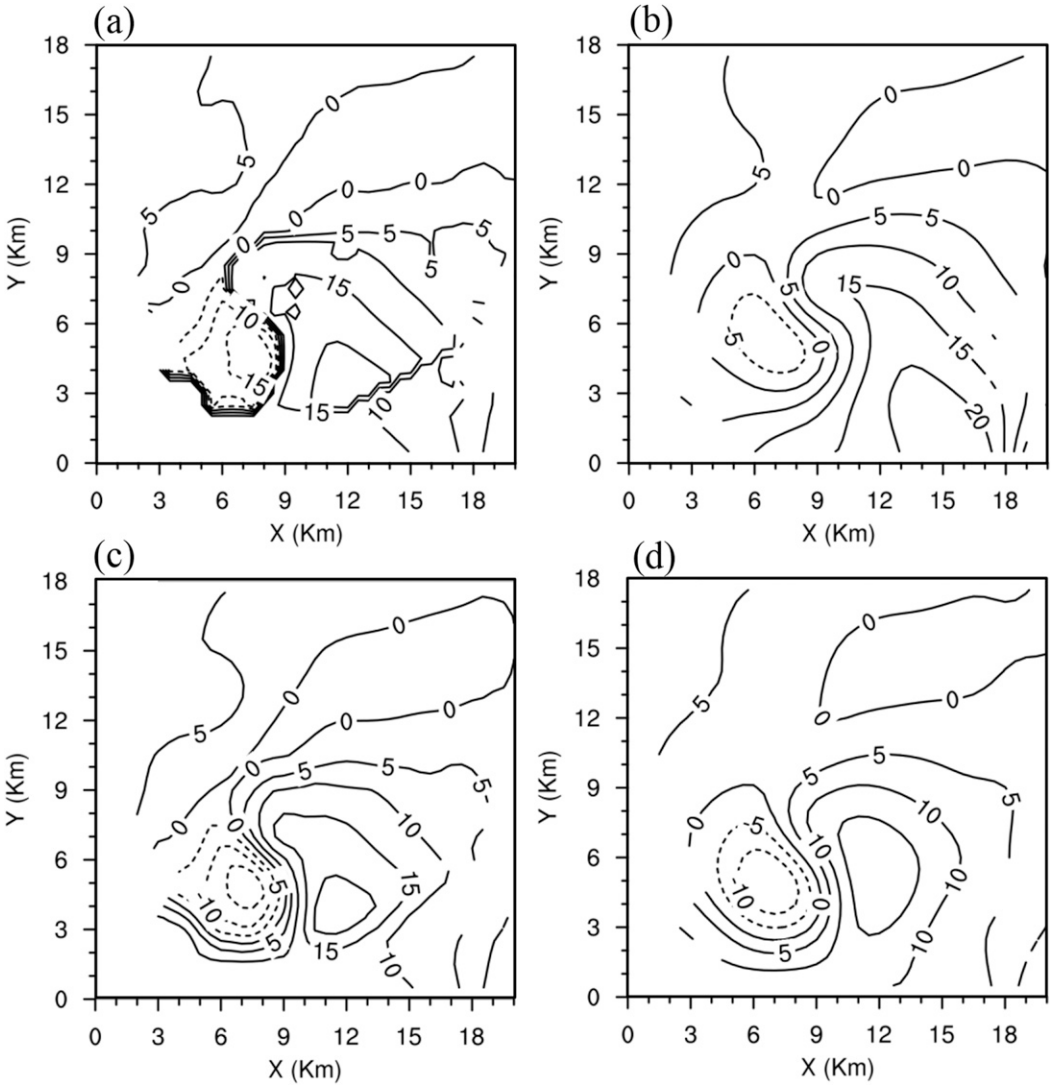

FIG. 6. The radial wind component viewed from the location of the MWR-05XP at $Z = 500$ m AGL obtained by (a) the raw radial wind observed by MWR-05XP, (b) dual-Doppler synthesis using DOW6 and DOW7, and SDVR by MWR-05XP data with (c) SDPA6s and (d) SDPA3m. Positive (negative) values are depicted by solid (dashed) contour lines with 5 m s^{-1} intervals.

regardless of the temporal resolution, SCC is always ~0.85. The SCC for the retrieved azimuthal wind with 6-s resolution can also reach as high as 0.8. However, when the temporal resolution is reduced to 3 min, the SCC for the retrieved V_{az} from SDPA3m drops to 0.5–0.6. Similar findings are depicted in Fig. 9, in which it can be seen that the RMSEs for the retrieved radial wind, with 6-s and 3-min resolutions, are both around 2.0–6.0 m s^{-1}. The RMSE for the retrieved azimuthal wind from SDPA6s is within the range of 5.0–7.0 m s^{-1}. However, the RMSEs of the retrieved V_{az} from SDPA3m increase to 9.0 m s^{-1} at low levels and are higher than those from SDPA6s at almost all altitudes, indicating a significant degradation in the quality of the retrieved azimuthal component. The aforementioned results are consistent with the conclusions of L02, in which a theoretical analysis indicates that the accuracy of the retrieved wind fields depends on the extent to which one can recover the azimuthal wind component, and the quality of the SDVR results can be improved by increasing the temporal resolution of the radar data.

5. Underestimation and overestimation of the wind speed

One major conclusion from L02 is that as a result of the discrete temporal nature of the radar data collection,

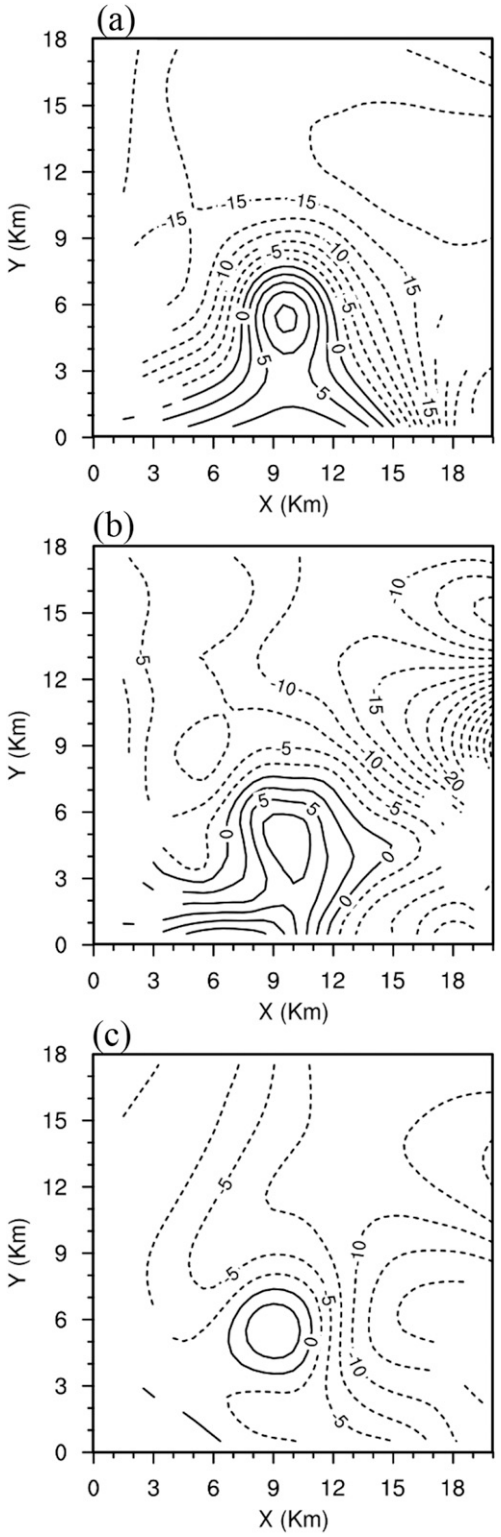

FIG. 7. The azimuthal wind component viewed from the location of the MWR-05XP at $Z = 500$ m AGL obtained by (a) dual-Doppler synthesis using DOW6 and DOW7, and SDVR by MWR-05XP data with (b) SDPA6s and (c) SDPA3m. Positive (negative) values are depicted by solid (dashed) contour lines with 2.5 m s^{-1} intervals.

the wind speed retrieved by a single-Doppler radar is always less than its true counterpart. This wind speed underestimation is more significant along the azimuthal component than the radial component. However, L02 also predicts that when the radar scan is rapid enough, overestimation of the azimuthal wind speed may happen. A brief explanation is provided below, while one can find more details in L02.

Using a simplified model, and assuming that the radar reflectivity possesses a sine waveform with an advection speed of u and wavelength λ, L02 [see his (14) and (17)] shows that the accuracy of the retrieved wind speed along the azimuthal component depends largely on parameter R', which is the ratio between the estimated wind speed based on temporally discrete data and the true wind speed, and is expressed as

$$R' = \left|\frac{\sin(2\pi\alpha\beta)}{\alpha\sin(2\pi\beta)}\right|, \tag{6a}$$

$$\alpha = \frac{u\Delta t}{\Delta x}, \tag{6b}$$

$$\beta = \frac{\Delta x}{\lambda}, \tag{6c}$$

where Δt and Δx stand for the temporal and spatial resolution of the radar data, respectively. When R' is less (greater) than 1.0, an underestimation (overestimation) of the azimuthal wind speed is implied, while $R' = 1$ represents a perfect wind speed retrieval.

By displaying the distribution of R' with respect to α and β, L02 (see his Fig. 1) illustrates that

$$\alpha\left(=\frac{u\Delta t}{\Delta x}\right) > 1.0 \quad R' < 1.0\,, \tag{7a}$$

$$\alpha\left(=\frac{u\Delta t}{\Delta x}\right) = 1.0 \quad R' = 1.0\,, \tag{7b}$$

$$\alpha\left(=\frac{u\Delta t}{\Delta x}\right) < 1.0 \quad R' > 1.0\,. \tag{7c}$$

Furthermore, the region with $R' < 1.0$ occupies a large portion of the plot, indicating that for most Δt and Δx used by modern, operational Doppler radars, α can easily exceed 1.0, leading to a wind speed underestimation [(7a)]. However, the same set of equations also suggests that if α can be effectively reduced to less than 1.0 by increasing the temporal resolution of the radar data (i.e., a sufficiently small Δt), then R' can be greater than 1.0, meaning an azimuthal wind speed overestimation is also possible [(7c)].

It should be noted that SDVR wind speed underestimation is frequently observed (e.g., Yang and Xu 1996; ZG96; Liou and Luo 2001; Lazarus et al. 2001). By contrast, the phenomenon of wind speed overestimation predicted by the analyses in L02 has not been verified.

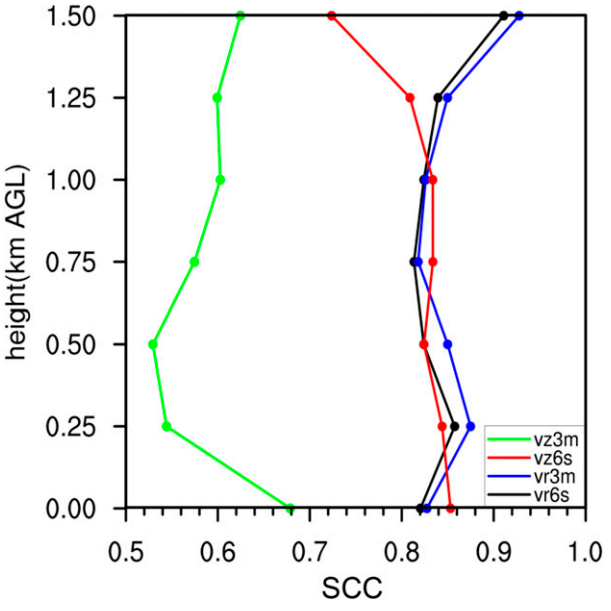

FIG. 8. Vertical profiles of the SCC values from 0.0 to 1.5 km AGL obtained from experiment SDPA6s for the radial wind (black) and azimuthal wind (red), and from experiment SDPA3m for the radial wind (blue) and azimuthal wind (green).

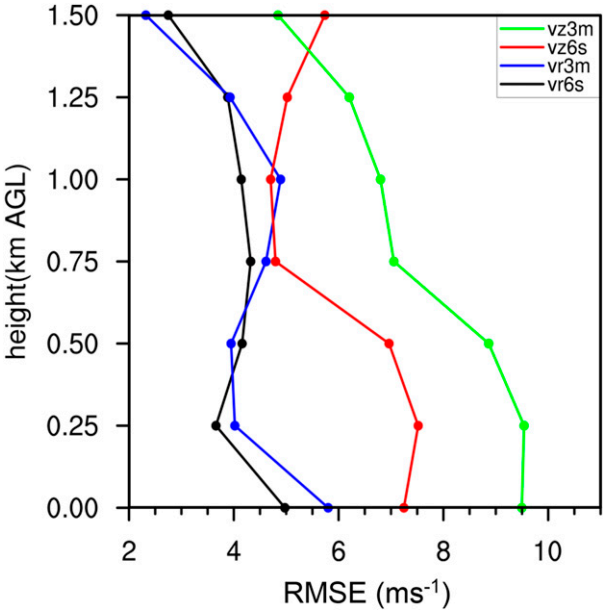

FIG. 9. As in Fig. 8, but vertical profiles of the RMSE values obtained from experiments SDPA6s and SDPA3m.

Thus, in this section we examine whether wind speed overestimation could actually occur when the data used for SDVR are collected by a rapid scan, phased-array radar with an extremely high sampling rate.

The difference of the wind speed (V_{diff}) is computed on each layer by

$$V_{\text{diff}} = \frac{1}{N}\sum(|V_{\text{sdvr}}| - |V_{\text{dual}}|), \tag{8}$$

where V can be either V_r or V_{az}; the subscripts "sdvr" and "dual" denote the wind components obtained by single-Doppler velocity retrieval and dual-Doppler synthesis, respectively; and N is the number of grid points. Thus, a positive (negative) V_{diff} indicates a wind speed overestimation (underestimation).

Figure 10 displays the vertical distribution of V_{diff}. For the retrieved radial wind component V_r from SDPA6s, only a minor underestimate is noted, with the maximum difference being less than $-1.0\,\text{m s}^{-1}$. If the temporal resolution is degraded from 6 s to 3 min, then the maximum underestimation of the radial wind from SDPA3m increases only slightly to $-1.7\,\text{m s}^{-1}$. For the retrieved azimuthal component V_{az} from SDPA3m, it is found that significant wind speed underestimation along the azimuthal direction takes place at all layers, with the maximum difference exceeding $-4.0\,\text{m s}^{-1}$. However, if the temporal resolution is increased to 6 s as in SDPA6s, then the wind speed underestimation is effectively mitigated. Moreover, the phenomenon of wind speed overestimation does occur in the lower and higher layers, with the magnitude reaching $2.5\,\text{m s}^{-1}$.

To show that the wind speed underestimation/overestimation is a phenomenon that takes place throughout the domain instead of at only a small portion of the points, Fig. 11 computes the ratio of the grid points on each horizontal layer where the retrieved azimuthal wind speed is underestimated. It is illustrated that when the temporal resolution of the data is 3 min (SDPA3m), the wind speed underestimation occurs at approximately 80% of the grid points on each layer. However, when the temporal resolution is increased to 6 s (SDPA6s), this ratio drops dramatically at all layers, implying an overall mitigation of the wind speed underestimation throughout the domain. At lower and higher layers, the ratio of grid points with underestimation is significantly below 0.5, indicating the feature of wind speed overestimation occurs at far more than half of the domain.

The aforementioned results demonstrate that the prediction of an overestimation of the retrieved azimuthal wind made by L02 in his theoretical analysis is verified by a set of real rapid scan data collected by a phased-array radar.

According to L02, the accuracy of the retrieved wind speed from SDVR depends not only on the radar sampling rate but also on the spatial resolution of the data, as well as on the intrinsic wavelength and flow speed of the targeted weather system. In other words, it would be difficult to determine an optimal scanning strategy suitable for all

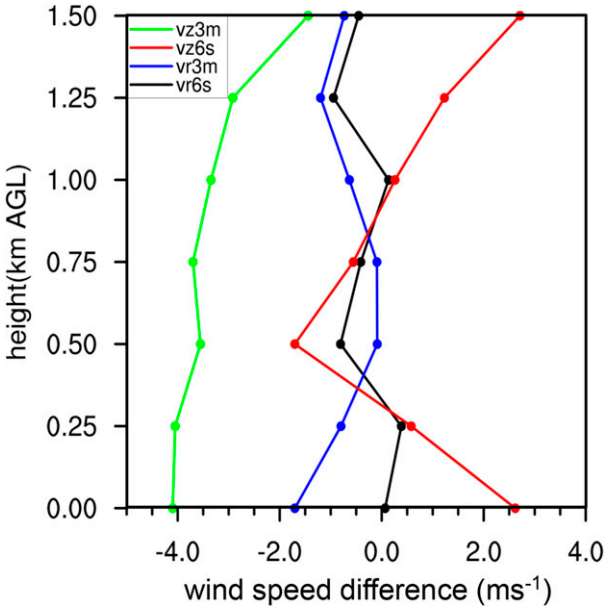

FIG. 10. As in Fig. 8, but vertical profiles of the wind speed difference obtained from experiments SDPA6s and SDPA3m. The negative (positive) number indicates a wind speed underestimation (overestimation).

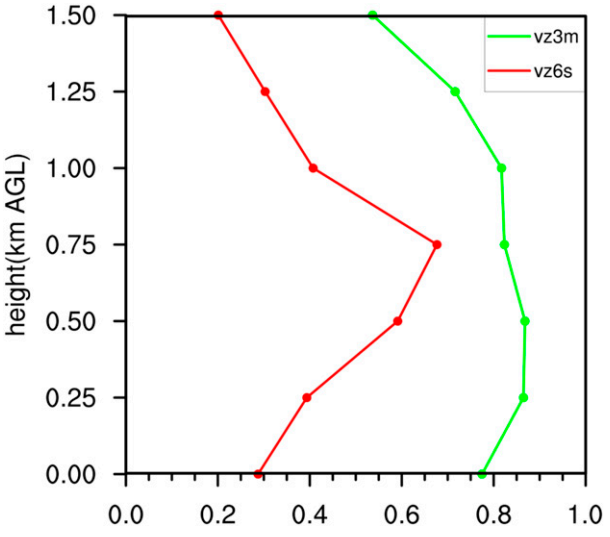

FIG. 11. Vertical profiles of the ratio of grid points on each horizontal plane where the azimuthal wind speed is underestimated. Results from experiments SDPA3m (green) and SDPA6s (red).

cases. Nevertheless, for the case studied in this research, it is demonstrated that the overall quality of the retrieved wind field can be improved significantly by increasing the radar sampling rate from 3 min to 6 s, and the wind speed overestimation caused by the extremely high temporal resolution is not serious. Based on these conclusions, it is suggested that for the purposes of a more accurate SDVR, faster scanning rates, such as those used by phased-array radars, be implemented when observing supercells and other rapid-evolving phenomena.

6. Necessity of using the optimal moving frame of reference

When the temporal radar sampling rate is too low, analyses based on radar observations are prone to errors. Previous studies (e.g., Gal-Chen 1982; Liou and Luo 2001; Shapiro et al. 2010a) have pointed out that this type of error can be reduced by using an advection-correction procedure, meaning that better products can be obtained if the computation is performed on an optimal moving frame of reference instead of a fixed reference. In this study the dataset used for the SDVR is from a phased-array radar with an extremely high sampling rate of 6 s per volume scan. One interesting question that arises is whether it is still necessary to apply the optimal moving frame strategy for SDVR. Therefore, the same experiment as in SDPA6s is used as a test, except that the retrieval is conducted without using the optimal moving frame of reference strategy. Figure 12 clearly shows that the retrieved wind field fails to capture the complete rotational structure in the hook-echo region. The flow field surrounding the mesocyclone is also poorly retrieved. Figure 13 depicts the SCC and RMSE for this experiment. It can be seen that the SCC value remains below 0.3, while the RMSE exceeds 7.0 m s^{-1} at all levels, with the maximum error reaching over 10.0 m s^{-1}. The overall quality of the retrieved wind field obtained in this experiment turns out to be much worse than that obtained from SDPA6s as shown in Figs. 8 and 9. Thus, we note the necessity of adopting an optimal moving frame of reference for SDVR, even though the data are from a phased-array radar capable of performing rapid scans.

7. Single-Doppler retrieval results using DOW6 and DOW7

To demonstrate the robustness of the single-Doppler retrieval scheme employed in this study, two more experiments are designed in which the data from DOW6 and DOW7 are used to perform SDVR. The temporal resolution of the datasets from these two radars is 2 min. Note that the tests in the previous sections represent experiments using radar data collected at the same geographic location but with different temporal resolutions. By contrast, this section presents the experimental results using radar data measured at two different locations but with the same temporal resolution.

The retrieved wind fields are displayed in Fig. 14, which can be compared against the dual-Doppler synthesized

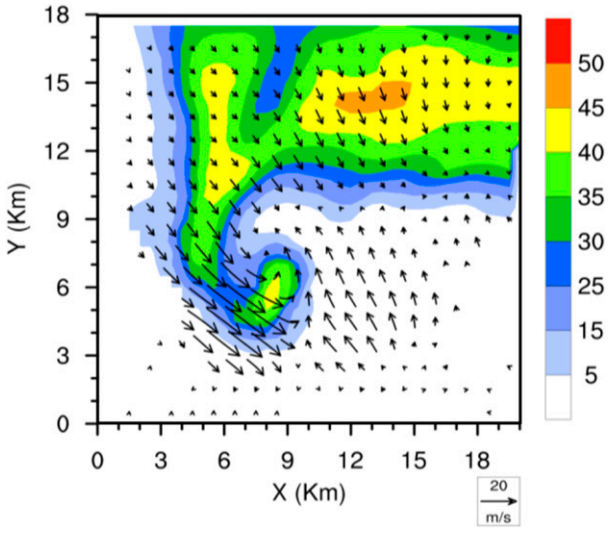

FIG. 12. The retrieved wind field using 6-s temporal resolution MWR-05XP radar data but without applying the optimal moving frame of reference. The color shading indicates the radar reflectivity.

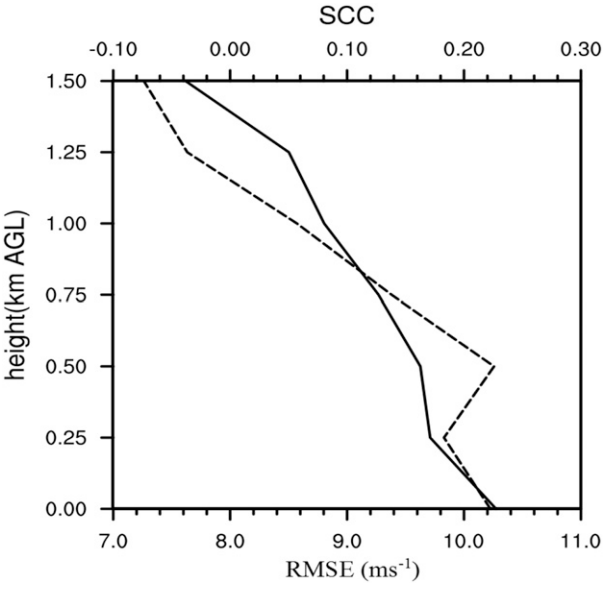

FIG. 13. The SCC (solid line) and RMSE (dashed line) from the SDVR experiment using 6-s temporal resolution MWR-05XP radar data but without applying the optimal moving frame of reference.

wind field depicted in Fig. 2a. The results show that by using data from either radar, even with poorer data temporal resolution than that of the 6-s phased-array radar data, the counterclockwise circulation of the mesocyclone in the hook-echo area can still be successfully recovered, though the details, such as the location of the rear-flank gust front retrieved by DOW7, are shifted eastward.

A quantitative assessment of the results is conducted by computing the SCC and RMSE for the retrieved radial and azimuthal wind components in a three-dimensional domain from the surface to $Z = 1.5$ km AGL. Table 1 indicates that by using DOW7 datasets, the retrievals are better than those by DOW6, as revealed by its higher SCC and smaller RMSE values, especially along the azimuthal wind component.

The DOW6 and DOW7 radars are located at two geographic locations; therefore, for a given wind field, the wind information measured by each radar is different. To quantify this difference, Liou and Luo (2001) computed the ratio of the unobservable azimuthal component to the observable radial component by defining an areawide-averaged index [azimuth over radial (AOR)] as

$$\mathrm{AOR} = \frac{\sqrt{\sum (V_{\mathrm{az}})^2}}{\sqrt{\sum (V_r)^2}}. \tag{9}$$

A small (large) AOR simply means that, from this radar site, the unknown azimuthal winds are generally weaker (stronger) than the observable radial winds. As a result, a better (worse) retrieval can be expected.

By using the radial and azimuthal wind fields obtained by the dual-Doppler synthesis, Table 1 shows that the AOR index from DOW7 is indeed lower than that from DOW6, implying that DOW7 is deployed at a favorable position, compared to DOW6, to observe the supercell. This explains the superiority of the SDVR results by the DOW7 radar for this particular case.

8. Summary

In this study a least squares–type SDVR algorithm is tested using data collected during VORTEX2 by a phased-array radar (MWR-05XP) and two mobile Doppler radars (DOW6 and DOW7) with the temporal resolution of the datasets being 6 s, 3 min. and 2 min, respectively. In all the experiments, the rotational flow of the mesocyclone in the hook-echo region is at least qualitatively well retrieved. An assessment of the quality of the SDVR results obtained from MWR-05XP confirms the conclusions from an earlier theoretical analysis by L02, that because of the temporarily discrete nature of the radar scans, the underestimation of the retrieved wind speed is mainly caused by the underestimation of the azimuthal wind speed. This underestimation can be effectively mitigated by increasing the temporal resolution of the radar data. Most importantly, when the radar scanning rate is fast enough, the prediction of L02 that even an overestimation of the azimuthal wind speed can happen is verified in this real

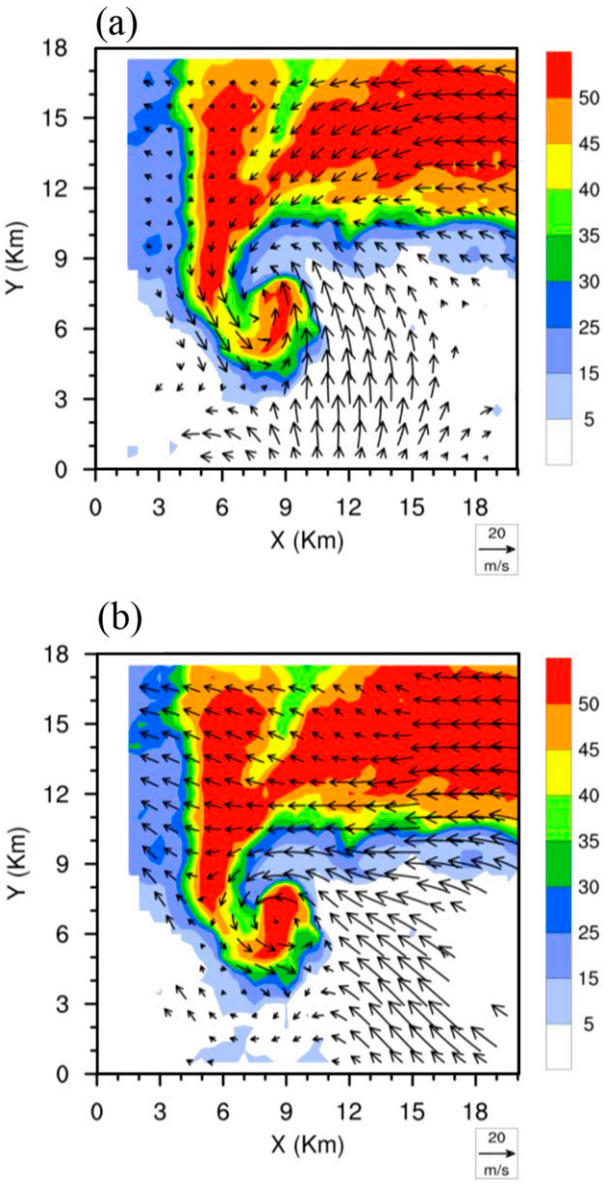

FIG. 14. The wind vectors at $Z = 500$ m AGL obtained using SDVR by (a) DOW6 and (b) DOW7 with 2-min temporal resolution data. The color shading indicates the radar reflectivity (dBZ).

case study. It is also demonstrated that the use of an optimal moving frame of reference for SDVR is necessary, even when the input data are collected by a rapid scan phased-array radar.

According to L02, the accuracy of the SDVR results depends on the sampling rate and the wind speed, as well as the ratio between the radar data spatial resolution and the spatial scale of the weather system. Therefore, it would be difficult to determine an optimal scanning rate suitable for all cases. Moreover, the SDVR experiments using DOW6 and DOW7 alone also reveal that the viewing angle from the radar to the target is another factor that can affect the accuracy of the SDVR results. Nevertheless, this study and L02 indicate that although low and high temporal resolutions could lead to underestimation and overestimation, respectively, the amount of over- and underestimation is different. The degree of the overestimation is found to be less significant than that of the underestimation. Thus, it is still the recommendation to use the highest scanning rate a radar can achieve when performing SDVR.

TABLE 1. The SCC and RMSE values computed by SDVR using DOW6 and DOW7 radar observations. The AOR index is defined in (9) in the text.

	SCC		RMSE ($m\,s^{-1}$)		
	V_r	V_{az}	V_r	V_{az}	AOR
DOW6	0.96	0.43	1.98	9.04	1.66
DOW7	0.97	0.75	1.46	7.20	1.16

The SDVR algorithm applied in this manuscript has been tested using idealized datasets and several real cases (e.g., Liou 1999; Liou and Luo 2001; L02; L07). The results obtained from previous research and this study indicate that this SDVR algorithm can perform reasonably well in retrieving horizontal winds, especially with rapid scan radar data. The retrieved vertical velocity field, however, should be interpreted at a qualitative sense. When multiple-Doppler observations are not available, SDVR can provide more information about the flow field, although its accuracy may not be as good as that from multiple-Doppler syntheses.

Acknowledgments. This research is supported by the Ministry of Science and Technology of Taiwan under MOST103-2119-M-008-008 and MOST103-2625-M-008-008-MY2. The second author has been funded by NSF Grants AGS-1262048 and AGS-1560945. The authors also wish to extend their gratitude to Mr. Chia-Yen Hsu, who helped to process the radar data; and to Mr. Po-Chien Yang, who prepared the figures. Bob Bluth at CIRPAS of the Naval Postgraduate School provided the MWR-05XP. The DOW data were collected by Josh Wurman and his group.

REFERENCES

Bluestein, H. B., M. M. French, I. PopStefanja, R. T. Bluth, and J. B. Knorr, 2010: A mobile, phased-array Doppler radar for the study of severe convective storms. *Bull. Amer. Meteor. Soc.*, **91**, 579–600, https://doi.org/10.1175/2009BAMS2914.1.

French, M. M., H. B. Bluestein, I. PopStefanja, C. A. Baldi, and R. T. Bluth, 2013: Reexamining the vertical development of tornadic vortex signature in supercells. *Mon. Wea. Rev.*, **141**, 4576–4601, https://doi.org/10.1175/MWR-D-12-00315.1.

——, ——, I. PopStefanja, C. A. Baldi, and R. T. Bluth, 2014: Mobile, phased-array, Doppler radar observations of tornadoes at X band. *Mon. Wea. Rev.*, **142**, 1010–1036, https://doi.org/10.1175/MWR-D-13-00101.1.

——, P. S. Skinner, L. J. Wicker, and H. B. Bluestein, 2015: Documenting a rare tornado merger observed in the 24 May 2011 El Reno–Piedmont, Oklahoma, Supercell. *Mon. Wea. Rev.*, **143**, 3025–3043, https://doi.org/10.1175/MWR-D-14-00349.1.

Gal-Chen, T., 1982: Errors in fixed and moving frame of reference: Applications for conventional and Doppler radar analysis. *J. Atmos. Sci.*, **39**, 2279–2300, https://doi.org/10.1175/1520-0469(1982)039<2279:EIFAMF>2.0.CO;2.

Gao, J.-D., M. Xue, A. Shapiro, Q. Xu, and K. K. Doregemeier, 2001: Three-dimensional simple adjoint velocity retrievals from single-Doppler radar. *J. Atmos. Oceanic Technol.*, **18**, 26–38, https://doi.org/10.1175/1520-0426(2001)018<0026:TDSAVR>2.0.CO;2.

——, ——, S.-Y. Lee, A. Shapiro, Q. Xu, and K. K. Droegemeier, 2006: A three-dimensional variational single-Doppler velocity retrieval method with simple conservation equation constraint. *Meteor. Atmos. Phys.*, **94**, 11–26, https://doi.org/10.1007/s00703-005-0170-7.

Laroche, S., and I. Zawadzki, 1994: A variational analysis method for retrieval of three-dimensional wind field from single-Doppler radar data. *J. Atmos. Sci.*, **51**, 2664–2682, https://doi.org/10.1175/1520-0469(1994)051<2664:AVAMFR>2.0.CO;2.

Lazarus, S., A. Shapiro, and K. Droegemeier, 1999: Analysis of the Gal-Chen–Zhang single-Doppler velocity retrieval. *J. Atmos. Oceanic Technol.*, **16**, 5–18, https://doi.org/10.1175/1520-0426(1999)016<0005:AOTGCZ>2.0.CO;2.

——, ——, and ——, 2001: Application of the Zhang–Gal-Chen single-Doppler velocity retrieval to a deep convective storm. *J. Atmos. Sci.*, **58**, 998–1016, https://doi.org/10.1175/1520-0469(2001)058<0998:AOTZGC>2.0.CO;2.

Lee, W.-C., and J. Wurman, 2005: Diagnosed three-dimensional axisymmetric structure of the Mulhall tornado on 3 May 1999. *J. Atmos. Sci.*, **62**, 2373–2393, https://doi.org/10.1175/JAS3489.1.

——, B. J.-D. Jou, P.-L. Chang, and S.-M. Deng, 1999: Tropical cyclones kinematic structure retrieved from single-Doppler radar observations. Part I: Interpretation of Doppler velocity patterns and the GBVTD technique. *Mon. Wea. Rev.*, **127**, 2419–2439, https://doi.org/10.1175/1520-0493(1999)127<2419:TCKSRF>2.0.CO;2.

Liou, Y.-C., 1999: Single radar recovery of cross-beam wind components using a modified moving frame of reference technique. *J. Atmos. Oceanic Technol.*, **16**, 1003–1016, https://doi.org/10.1175/1520-0426(1999)016<1003:SRROCB>2.0.CO;2.

——, 2002: An explanation of the wind speed underestimation obtained from a least squares type single-Doppler radar velocity retrieval method. *J. Appl. Meteor.*, **41**, 811–823, https://doi.org/10.1175/1520-0450(2002)041<0811:AEOTWS>2.0.CO;2.

——, 2007: Single-Doppler retrieval of the three-dimensional wind in a deep convective system based on an optimal moving frame of reference. *J. Meteor. Soc. Japan*, **85**, 559–582, https://doi.org/10.2151/jmsj.85.559.

——, and I.-S. Luo, 2001: An investigation of the moving-frame single-Doppler wind retrieval technique using Taiwan Area Mesoscale Experiment low-level data. *J. Appl. Meteor.*, **40**, 1900–1917, https://doi.org/10.1175/1520-0450(2001)040<1900:AIOTMF>2.0.CO;2.

——, and Y.-J. Chang, 2009: A variational multiple–Doppler radar three-dimensional wind synthesis method and its impacts on thermodynamic retrieval. *Mon. Wea. Rev.*, **137**, 3992–4010, https://doi.org/10.1175/2009MWR2980.1.

——, S.-F. Chang, and J. Sun, 2012: An application of the immersed boundary method for recovering the three-dimensional wind fields over complex terrain using multiple-Doppler radar data. *Mon. Wea. Rev.*, **140**, 1603–1619, https://doi.org/10.1175/MWR-D-11-00151.1.

——, T.-C. Chen Wang, and P.-Y. Huang, 2016: The inland eyewall re-intensification of Typhoon Fanapi (2010) documented from an observational perspective using multiple-Doppler radar and surface measurements. *Mon. Wea. Rev.*, **144**, 241–261, https://doi.org/10.1175/MWR-D-15-0136.1.

Markowski, P., and Coauthors, 2012: The pretornadic phase of the Goshen County, Wyoming, supercell of 5 June 2009 intercepted by VORTEX2. Part I: Evolution of kinematic and surface thermodynamic fields. *Mon. Wea. Rev.*, **140**, 2887–2915, https://doi.org/10.1175/MWR-D-11-00336.1.

Qiu, C., and Q. Xu, 1992: A simple adjoint method of wind analysis for single-Doppler data. *J. Atmos. Oceanic Technol.*, **9**, 588–598, https://doi.org/10.1175/1520-0426(1992)009<0588:ASAMOW>2.0.CO;2.

——, and ——, 1996: Least squares retrieval of microburst winds from single-Doppler radar data. *Mon. Wea. Rev.*, **124**, 1132–1144, https://doi.org/10.1175/1520-0493(1996)124<1132:LSROMW>2.0.CO;2.

——, A. M. Shao, S. Liu, and Q. Xu, 2006: A two-step variational method for three-dimensional wind retrieval from single-Doppler radar. *Meteor. Atmos. Phys.*, **91**, 1–8, https://doi.org/10.1007/s00703-004-0093-8.

Qiu, X., Q. Xu, C. Qiu, K. Nai, and P. Zhang, 2013: Retrieving 3D wind field from phased array radar rapid scans. *Adv. Meteor.*, **2013**, 792631, https://doi.org/10.1155/2013/792631.

Shapiro, A., S. Ellis, and J. Shaw, 1995: Single-Doppler velocity retrievals with Phoenix II data: Clear air and microburst wind retrievals in the planetary boundary layer. *J. Atmos. Sci.*, **52**, 1265–1287, https://doi.org/10.1175/1520-0469(1995)052<1265:SDVRWP>2.0.CO;2.

——, P. Robinson, J. Wurman, and J. Gao, 2003: Single-Doppler velocity retrieval with rapid-scan radar data. *J. Atmos. Oceanic Technol.*, **20**, 1758–1775, https://doi.org/10.1175/1520-0426(2003)020<1758:SVRWRR>2.0.CO;2.

——, C. K. Potvin, and J. Gao, 2009: Use of a vertical vorticity equation in variational dual-Doppler wind analysis. *J. Atmos. Oceanic Technol.*, **26**, 2089–2106, https://doi.org/10.1175/2009JTECHA1256.1.

——, K. M. Willingham, and C. K. Potvin, 2010a: Spatially variable advection correction of radar data. Part I: Theoretical considerations. *J. Atmos. Sci.*, **67**, 3445–3456, https://doi.org/10.1175/2010JAS3465.1.

——, ——, and ——, 2010b: Spatially variable advection correction of radar data. Part II: Test results. *J. Atmos. Sci.*, **67**, 3457–3470, https://doi.org/10.1175/2010JAS3466.1.

Sun, J., D. K. Flicker, and D. K. Lilly, 1991: Recovery of three-dimensional wind and temperature fields from simulated Doppler radar data. *J. Atmos. Sci.*, **48**, 876–890, https://doi.org/10.1175/1520-0469(1991)048<0876:ROTDWA>2.0.CO;2.

Tanamachi, R. L., H. B. Bluestein, W.-C. Lee, M. Bell, and A. Pazmany, 2007: Ground-based velocity track display (GBVTD) analysis of W-band Doppler radar data in a tornado near Stockton, Kansas, on 15 May 1999. *Mon. Wea. Rev.*, **135**, 783–800, https://doi.org/10.1175/MWR3325.1.

Weygandt, S. S., A. Shapiro, and K. K. Droegemeier, 2002: Retrieval of model initial fields from single-Doppler observations of a supercell thunderstorm. Part I: Single-Doppler Velocity Retrieval. *Mon. Wea. Rev.*, **130**, 433–453, https://doi.org/10.1175/1520-0493(2002)130<0433:ROMIFF>2.0.CO;2.

Wurman, J., D. Dowell, Y. Richardson, P. Markowski, E. Rasmussen, D. Burgess, L. Wicker, and H. B. Bluestein, 2012: The second

Verification of the Origins of Rotation in Tornadoes Experiment: VORTEX2. *Bull. Amer. Meteor. Soc.*, **93**, 1147–1170, https://doi.org/10.1175/BAMS-D-11-00010.1.

Xu, Q., C.-J. Qiu, and J.-X. Yu, 1994: Adjoint-method retrievals of low-altitude wind fields from single-Doppler wind data. *J. Atmos. Oceanic Technol.*, **11**, 579–585, https://doi.org/10.1175/1520-0426(1994)011<0579:AMROLA>2.0.CO;2.

——, ——, H.-D. Gu, and J.-X. Yu, 1995: Simple adjoint retrievals of microburst winds from single-Doppler radar data. *Mon. Wea. Rev.*, **123**, 1822–1833, https://doi.org/10.1175/1520-0493(1995)123<1822:SAROMW>2.0.CO;2.

Yang, S., and Q. Xu, 1996: Statistical errors in variational data assimilation—A theoretical one-dimensional analysis applied to Doppler wind retrieval. *J. Atmos. Sci.*, **53**, 2563–2577, https://doi.org/10.1175/1520-0469(1996)053<2563:SEIVDA>2.0.CO;2.

Zhang, J., and T. Gal-Chen, 1996: Single-Doppler wind retrieval in the moving frame of reference. *J. Atmos. Sci.*, **53**, 2609–2623, https://doi.org/10.1175/1520-0469(1996)053<2609:SDWRIT>2.0.CO;2.